Chemical Physics Letters 804 (2022) 139887

Contents lists available at ScienceDirect

Chemical Physics Letters

journal homepage: www.elsevier.com/locate/cplett

Research paper

Temperature-dependent bandgap of (In,Ga)As via ***P5Grand***: A ***P***ython ***P***ackage for ***P***roperty ***P***rediction of ***P***seudobinary systems using ***Grand*** canonical ensemble

Gyuseung Han [a,b], In Won Yeu [a], Kun Hee Ye [a,b], Seungjae Yoon [a,b], Taeyoung Jeong [a,b], Seung-Cheol Lee [c], Cheol Seong Hwang [b], Jung-Hae Choi [a,*]

[a] Electronic Materials Research Center, Korea Institute of Science and Technology, Seoul 02792, Republic of Korea
[b] Department of Materials Science and Engineering and Inter-University Semiconductor Research Center, Seoul National University, Seoul 08826, Republic of Korea
[c] Indo-Korea Science and Technology Center, Bengaluru 560065, India

ARTICLE INFO

Keywords:
(InGa)As solid solution
Temperature-dependent bandgap
Configuration-dependent bandgap
Ab initio thermodynamics
Python package

ABSTRACT

We introduce introduces an open-source program for calculating the properties of solid solutions, "***P***ython ***P***ackage for ***P***roperty ***P***rediction of ***P***seudobinary systems using ***Grand*** canonical ensemble" (***P5Grand***). ***P5Grand*** uses two main strategies to improve calculation efficiency: random configuration sampling and separate calculations of the strain energy induced by local compositional fluctuations within the grand canonical ensemble. ***P5Grand*** can efficiently calculate thermodynamic properties and any properties of interest for arbitrary solid solution as a function of temperature and composition using two input files. The efficiency of ***P5Grand*** is demonstrated by the bandgap prediction of (In,Ga)As.

1. Introduction

Solid solutions, such as A_xB_{1-x} or $(A_xB_{1-x})C$, provide versatile control of material properties. For example, the III-V pseudobinary solid solution of (In,Ga)As has been studied to obtain optimal properties for its use as a semiconductor channel or an optoelectronic material [1,2]. Recently, various III-V pseudobinary semiconductors, cation solid solutions, such as (In,Ga)N and (Al,Ga)P, and anion solid solutions, such as Ga(As,Sb) and In(As,P), have been used to modulate lattice constants and bandgaps (E_g) [2–4]. The ability to predict composition-dependent properties through simulation is crucial for efficient material design because of the wide range of combinatorial compositions. However, the nonperiodicity and broken symmetry of solid solutions make it challenging to calculate the property of interest (PoI) using density functional theory (DFT). The special quasi-random structure [5] and deep neural network potential [6–8] have been used to obtain the PoIs of solid solutions.

Recently, the authors reported two theoretical studies on the prediction of the phase diagram [9] and bandgap [4] of III–V pseudobinary materials based on *ab initio* thermodynamics using the following steps: (i) DFT calculation of the energetics and bandgap of individual configurations (σ), (ii) extraction of the effective cluster interaction (ECI) coefficients using the cluster expansion (CE) method, and (iii) prediction of the ensemble-averaged thermodynamic properties and bandgap using the grand canonical ensemble (μVT). The grand canonical approach considers local compositional fluctuations, making it appropriate for studying solid solution properties. The local fluctuation of a composition in the grand canonical ensemble induces strain, which is referred to as a local strain. It has been mathematically demonstrated that it is necessary to consider this local strain energy for phase separation to occur [9]. In addition, the local strain energy of (In,Ga)As has been confirmed to be well fitted to a single Birch–Murnaghan equation of state (B–M EOS) regardless of the configuration [9]. This means that it is not necessary to calculate the strain energy of individual configurations. Instead, the local strain energy can be calculated separately and then added to the energies of freely relaxed configurations, significantly reducing computation costs.

This paper describes an open-source package, the ***P***ython ***P***ackage for ***P***roperty ***P***rediction of ***P***seudobinary systems using ***Grand*** canonical ensemble (***P5Grand***), which implements the abovementioned methodology and facilitates the efficient prediction of properties for various pseudobinary systems. It predicts thermodynamic properties (such as

* Corresponding author.
E-mail address: choijh@kist.re.kr (J.-H. Choi).

https://doi.org/10.1016/j.cplett.2022.139887
Received 5 May 2022; Received in revised form 27 June 2022; Accepted 18 July 2022
Available online 22 July 2022

free energy and phase diagram) and the ensemble average values of PoIs (such as bandgap and dielectric constant), starting from the atomistic property-configuration relations. For example, the bandgap prediction of $In_xGa_{1-x}As$ was used to demonstrate the applicability of ***P5Grand*** in this study. ***P5Grand*** predicts the average bandgap for a particular composition (x) and temperature (T) within the grand canonical ensemble based on the bandgap and energy of numerous configurations calculated using a combination of the DFT and CE methods. Although the use of ***P5Grand*** reduces the total computation cost, the calculated average bandgap of $In_xGa_{1-x}As$ is comparable to the experimental bandgap. The modular approach of ***P5Grand*** makes it easy to execute and suitable for extending its applicability beyond bandgaps and energy; ***P5Grand*** allows users to predict arbitrary PoIs as a function of x and T, using user inputs.

2. Description of *P5Grand*

P5Grand is an open-source code that automatically calculates the thermodynamic properties and ensemble average values of PoIs for pseudobinary systems. The code and manual of ***P5Grand*** are available to all users at URL website https://p5grand.readthedocs.io/en/latest/. ***P5Grand*** features three calculation modes: free energy mode, phase diagram mode, and PoI mode. As schematically shown in the workflow in Fig. 1 and the architecture in Fig. A1, the overall ***P5Grand*** package consists of four modules and one script: the "read," "grand_canonical_ensemble," "local_strain," and "analysis" modules and the "tool" script. The role of each module in the workflow is as follows: (i) the read module reads input files and selects one of the three calculation modes based on user commands; (ii) the grand_canonical_ensemble and local_strain modules calculate the grand canonical partition function and the local strain energy, respectively, which are required for subsequent calculations regardless of the calculation mode; and (iii) the analysis module performs property calculations based on the calculation mode, prints the properties (free energy and average PoI) as a function of composition, and plots a graph for the phase diagram depicting the binodal and spinodal points for the designated temperatures (see output examples in Fig. A2). The tool script is not essential, but it is useful in the ***P5Grand*** workflow because it generates an input file containing strain energy parameters in the required format. The tool script is described in detail below.

P5Grand requires two input files that can be generated using either DFT-based calculations or empirical-based data. The first file is called "*input file I,*" which contains a list of configuration properties, of which the format is determined by the calculation modes. It consists of two columns and many rows for the free energy and phase diagram modes (see Fig. A3(a)), where the first and second columns present the composition (x) and energy (E_σ) of a certain configuration (σ), while each row corresponds to each configuration. However, *input file I* for the PoI mode (see Fig. A3(b)) consists of three columns and many rows, with each column presenting the x, E_σ, and PoI of a certain configuration, such as a bandgap ($E_{g,\sigma}$).

P5Grand uses a fitting equation to treat the strain energy in order to reduce the total computational cost. The other input file, "*input file II,*" contains the fitting parameters for the strain energy. The current version of ***P5Grand*** provides a set of fitting parameters only for the B–M EOS [10] as a default setting:

$$E^{strain} = \frac{9V_0B_0}{16}\left\{\left[\left(\frac{V_0}{V}\right)^{\frac{2}{3}}-1\right]^3 B_0^{'} + \left[\left(\frac{V_0}{V}\right)^{\frac{2}{3}}-1\right]^2\left[6-4\left(\frac{V_0}{V}\right)^{\frac{2}{3}}\right]\right\} \quad (1)$$

where B_0 and $B_0^{'}$ are the bulk modulus and its derivative, and V_0 and V are the freely relaxed volume and the volume under isotropic strain, respectively. This is based on the authors' previous work in which the strain energy of (In,Ga)As was well fitted to a single B–M EOS regardless of the composition and configuration [9], and V_0 of (In,Ga)As was simply obtained using the lattice constant and Vegard's rule [9,11–13]. It should be noted that the composition- and configuration-independent strain energy curve was also confirmed in another III-V pseudobinary system, Ga(As,Sb) [9]. However, before executing ***P5Grand***, it is necessary to confirm that the strain energy of the pseudobinary system under investigation satisfies the default setting. The tool script extracts the fitting parameters of the local strain from the OUTCAR file of the Vienna Ab-initio Simulation Package (VASP) [14,15] and automatically writes them in *input file II* in the format shown in Fig. A3 (c). The B–M EOS is also the default equation in the tool script. The fitting equations in the local_strain module and the tool script can be manually modified by user, and they will be updated to account for composition-dependent cases.

P5Grand calculates the average PoI ($\overline{Y}$) at non-zero temperature using the following equation:

$$\overline{Y} = \sum_{\sigma} Y_\sigma P_\sigma \quad (2)$$

where P_σ is the probability that each configuration (σ) will occur in a

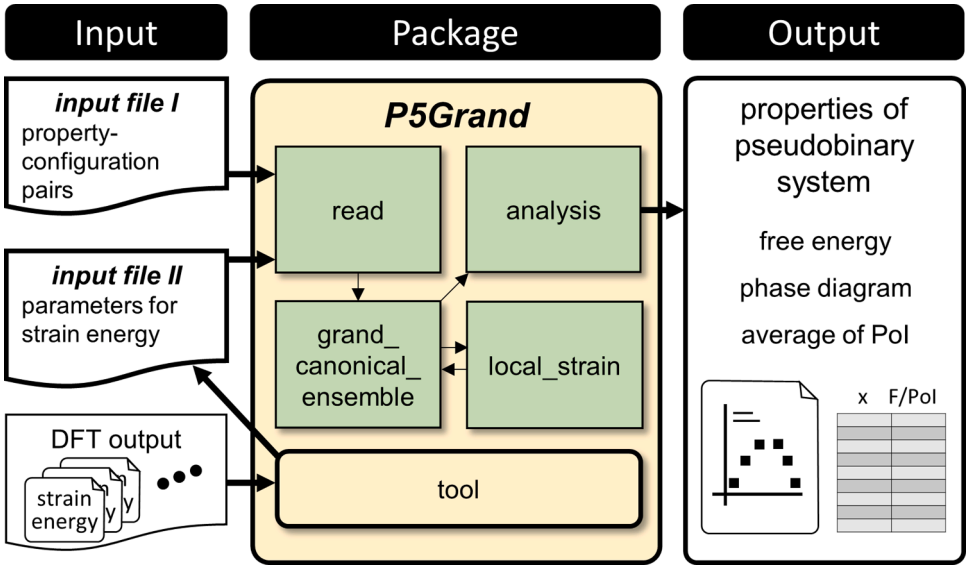

Fig. 1. Schematic overview on the workflow of ***P5Grand***.

pseudobinary system, $A_xB_{1-x}C$, and Y_σ is the PoI of σ. P_σ is calculated using the following equations:

$$P_\sigma = \frac{\exp\left(\frac{n_\sigma \Delta\mu - \Delta E_\sigma^{total}}{k_B T}\right)}{\mathbb{Z}(x,T)} \tag{3}$$

$$\mathbb{Z}(x,T) = \sum_\sigma \exp\left(\frac{n_\sigma \Delta\mu - \Delta E_\sigma^{total}}{k_B T}\right) \tag{4}$$

$$\Delta E_\sigma^{total} = \Delta E_\sigma + E^{strain} \tag{5}$$

$$\Delta E_\sigma = E_\sigma - [x_\sigma E_{AC} + (1 - x_\sigma) E_{BC}] \tag{6}$$

where $\mathbb{Z}(x,T)$ represents the grand partition function, k_B is the Boltzmann constant, T is the absolute temperature, and n_σ is the number of atom A in a configuration σ. When the sum of the number of atoms A and B is defined as N, the number of atom B in σ is $N - n_\sigma$, and the composition of σ (x_σ) is equal to n_σ/N; ΔE_σ^{total}, which is defined as Eq. (5), represents the total mixing energy. The first term of Eq. (5) (i.e., ΔE_σ) is the mixing energy for the pseudobinary system $A_xB_{1-x}C$, as shown in Eq. (6), where E_σ, E_{AC}, and E_{BC} are the freely relaxed energies of σ, AC, and BC, respectively. The second term of Eq. (5) (i.e., E^{strain}) is the local strain energy, which is induced by the local compositional fluctuation allowed in the grand canonical ensemble. The $\Delta\mu = \mu(A) - \mu(B)$ in Eq. (4) represents the difference in chemical potential between atoms A and B. Sometimes, it was calculated based on experimental conditions [16]. In this study, however, $\Delta\mu$ is determined for a given composition (x) using the bisection method to satisfy the self-consistency of Eq. (7) without experimental data.

$$x = \frac{1}{N}\sum_\sigma n_\sigma P_\sigma = \frac{1}{N}\sum_\sigma n_\sigma \frac{\exp\left(\frac{n_\sigma \Delta\mu - \Delta E_\sigma^{total}}{k_B T}\right)}{\mathbb{Z}(x,T)} \tag{7}$$

When Y_σ corresponds to ΔE_σ^{total}, the configurational entropy and free energy are calculated as Eqs. (8) and (9).

$$S(x) = -k_B \sum_\sigma P_\sigma \ln(P_\sigma) \tag{8}$$

$$\Delta F = \overline{\Delta E^{total}} - T\Delta S = Nx\Delta\mu - k_B T \ln \mathbb{Z}(x,T) \tag{9}$$

It is worth noting that ***P5Grand*** only considers configurational entropy.

Eq. (4) generally assumes that all possible configurations are calculated. However, in practice, it is impossible to calculate the energies of all possible configurations. Thus, ***P5Grand*** calculates the properties of a subset of configurations that are randomly sampled in each composition. When the properties of $K'_{n/N}$ configurations are specified among K possible configurations in the local composition n/N, the grand partition function is calculated as follows:

$$\mathbb{Z}(x,T) = \sum_{n=0}^{N}\left[\exp\left(\frac{n\Delta\mu - E^{strain}_{\sigma(n_\sigma=n)}}{k_B T}\right)\sum_{\sigma(n_\sigma=n)}\exp\left(\frac{-\Delta E_\sigma}{k_B T}\right)\frac{K_{n/N}}{K'_{n/N}}\right] \tag{10}$$

where $E^{strain}_{\sigma(n_\sigma=n)}$ is the strain energy of the configuration with n_σ equal to n. The $K'_{n/N}$ in the denominator in Eq. (10) implies that at least one configuration must be calculated at each possible n/N. The number of all possible configurations at n/N ($K_{n/N}$) is calculated as Eq. (11).

$$K_{n/N} = {}_NC_n = \frac{N!}{n!(N-n)!} \tag{11}$$

Details of the above equations are fully described in the authors' previous report [9]. When a phase transition is anticipated or atoms move away from their symmetric positions at high temperatures, the free energy and PoI can be calculated at each structure and compared. One of the alternative could be using machine learning potentials [6–8].

3. Application example of *P5Grand* and discussion

The average bandgaps $\overline{E_g}$ of $In_xGa_{1-x}As$ in a zinc-blende structure are calculated as a function of x for various T to demonstrate the property prediction of pseudobinary systems using ***P5Grand***. Before the ***P5Grand*** package is presented in this study, it should be noted that the methodology implemented in ***P5Grand*** accurately predicted the phase diagram of $In_xGa_{1-x}As$ [9].

The $E_{g,\sigma}$, E_σ, and E^{strain} are required to predict $\overline{E_g}$ using the PoI mode of ***P5Grand*** and they can be accurately obtained by DFT calculations. However, it is difficult to apply DFT to many configurations because of its high computational cost. Therefore, $E_{g,\sigma}$ and E_σ were calculated using a combination of DFT and CE methods. All DFT calculations were performed using the VASP [14,15]. The electron-core interaction was treated using Blöchl's projector augmented wave (PAW) approach [17,18]. The 4 × 4 × 4 k-points were sampled based on Γ-centered grid scheme for zinc-blende conventional unit cell. The cutoff energy was set at 500 eV. The experimental bandgaps were reproduced using the Heyd–Scuseria–Ernzerhof (HSE06) hybrid functional and a Hartree–Fock mixing parameter (α) of 0.25 [19]. In this study, E_g was calculated as 0.35 eV and 1.29 eV for InAs and GaAs, respectively, while the experimental E_g was reported as 0.36 eV and 1.43 eV for InAs and GaAs, respectively [12].

First, DFT calculations were performed to obtain E_σ and $E_{g,\sigma}$ for 30 configurations of $In_xGa_{1-x}As$ with a zinc-blende structured 2 × 2 × 2 supercell. The ECI coefficients were extracted from these $E_{g,\sigma}$ and E_σ values using the CE method. The ECI coefficient represents the contribution of the interaction between a group of k atoms (called a k-site cluster) to a PoI. In this study, the CE method was performed using the Lattice Configuration Simulation (LACOS) package with the following expressions [20]:

$$E_{g,\sigma} = \sum_k \sum_m J^{E_g}_{k,m} \overline{\prod_{\{i\}\in(k,m)} \theta(\sigma_i)} \tag{12}$$

$$E_\sigma = N \sum_k \sum_m J^{E}_{k,m} \overline{\prod_{\{i\}\in(k,m)} \theta(\sigma_i)} \tag{13}$$

where N is the number of cation sites (32 in the 2 × 2 × 2 supercell), $J^{E_g}_{k,m}$ and $J^{E}_{k,m}$ are the ECI coefficients for the bandgap and energy, $\{i\}$ is the symmetrically identical set of sites that make up the m^{th} k-site cluster (k, m), and $\theta(\sigma_i)$ is a function that returns − 1 for In atoms and 1 for Ga atoms according to the element occupying site i, σ_i. The orthogonal matching pursuit method implemented in the LACOS package was used to calculate the ECI coefficient. Fig. 2 (a) and (b) show the $J^{E_g}_{k,m}$ and $J^{E}_{k,m}$ obtained from the DFT results, and Fig. 2(c) shows the corresponding clusters. The low cross-validation (CV) scores for both E_g (12 meV) and ΔE (1.7 meV/atom) indicate that $J^{E_g}_{k,m}$ and $J^{\Delta E}_{k,m}$ are well optimized.

The properties of 10,000 configurations for every composition at an interval of 0.03125 (=1/32) in the 2 × 2 × 2 supercell were evaluated using the ECI coefficients obtained in Fig. 2(a) and (b), totaling 330,000 configurations (10,000 configurations for each composition). The results are plotted in Fig. 3. The x and y coordinates of each data point denote $\Delta E_\sigma/2N$ and $E_{g,\sigma}$ for each configuration, where N is 32 in this case. Since N is the number of cation sites in the 2 × 2 × 2 supercell of a zinc-blende structure, $\Delta E_\sigma/2N$ is the energy per atom. Furthermore, the color of each dot indicates the composition, which ranges from red for GaAs to violet for InAs. Even in a fixed composition with the same colors, $\Delta E_\sigma/2N$ and $E_{g,\sigma}$ vary depending on the configuration. For a given composition, a configuration with a lower ΔE_σ tends to have a higher $E_{g,\sigma}$, which becomes increasingly apparent as the composition becomes closer to GaAs. This tendency is because the magnitude of the ECIs in the two-site clusters is larger than that in the many-body clusters, and the signs of $J^{E_g}_{k,m}$ and $J^{E}_{k,m}$ are opposite for all two-site clusters in Fig. 2(a) and (b).

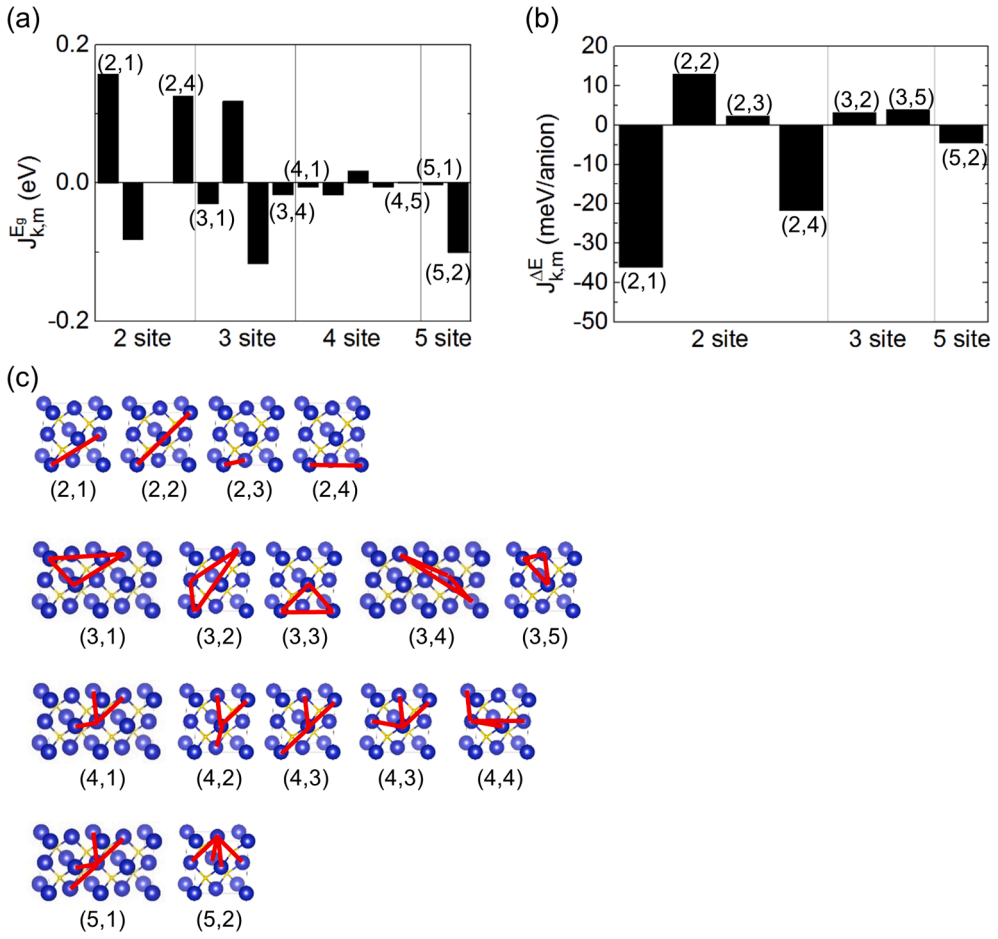

Fig. 2. Calculated ECIs and corresponding clusters. ECIs of (a) bandgap, (b) mixing energy of $In_xGa_{1-x}As$, and (c) corresponding clusters. The set of numbers (k,m) denotes m-th k-site cluster.

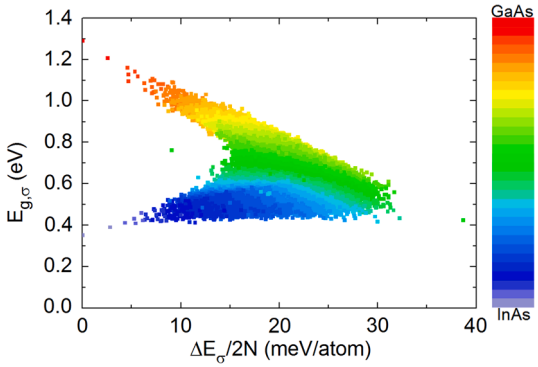

Fig. 3. Configuration-dependent bandgap and energy. Each colored data point represents the bandgap and mixing energy of the individual configuration. The color of each point denotes the composition x and 2 *N* is the total number of atoms in a 2 × 2 × 2 supercell.

However, the relationship between ΔE_σ and $E_{g,\sigma}$ is much weaker than that observed in the anionic pseudobinary system $GaAs_xSb_{1-x}$ in the authors' previous work [4]. The weak relationship is implied by $J^{E_g}_{2,m}$ having smaller absolute values in $In_xGa_{1-x}As$ than in $GaAs_xSb_{1-x}$. The composition (x_σ), energy (E_σ), and bandgaps ($E_{g,\sigma}$) of the 330,000 configurations were included in the first, second, and third columns of *input file I*.

On the other hand, the strain energy (E^{strain}) was calculated using DFT for a few representative compositions (x_σ) = 0, 0.25, 0.5, 0.75, and 1 in the zinc-blende unit cell, as shown in Fig. 4. The left y-axis represents the local strain energy per microstate, whereas the right y-axis represents the local strain energy per 2 *N*. The strain energy parameters were written in *input file II* and were well fitted to a single B–M EOS regardless of composition. The B_0 values were calculated as 57.3 GPa for InAs and 71.3 GPa for GaAs, which are in good agreement with the experimental values, 60.0 GPa for InAs and 74.8 GPa for GaAs [21].

The average bandgap ($\overline{E_g}$) at 300, 600, and 900 K and the infinite temperature were calculated as a function of the average composition x of $In_xGa_{1-x}As$ using the specified *input file I* and *input file II*, as indicated by colored solid lines in Fig. 5 (a), in comparison to the conventionally

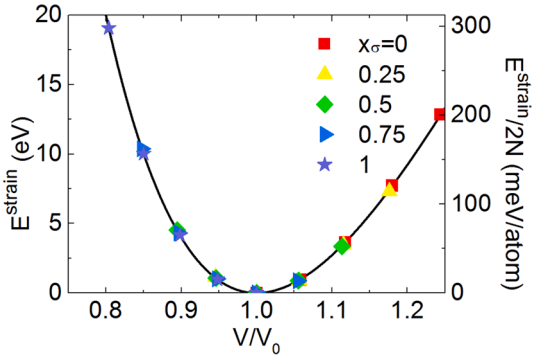

Fig. 4. Strain energy as a function of the relative volume V/V_0. The symbols denote the unit cell of $In_xGa_{1-x}As$ with various relative volumes, and the black curve is fitted to the Birch-Murnaghan equation of state.

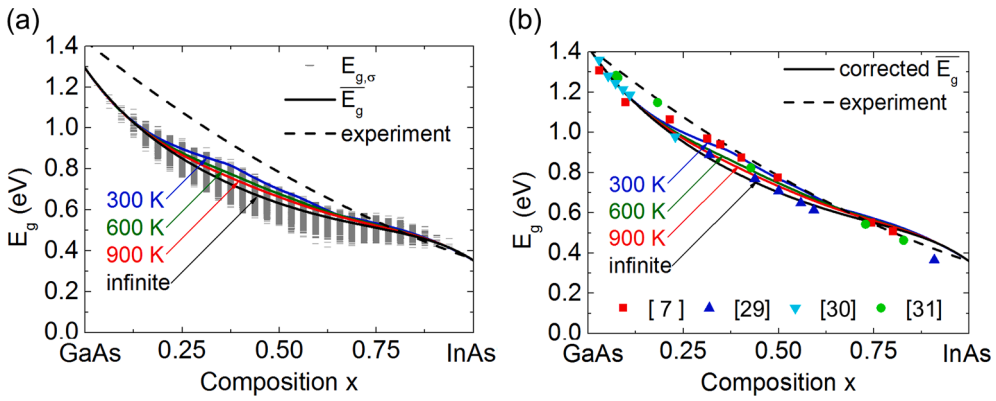

Fig. 5. (a) Calculated bandgap and (b) corrected bandgap of $In_xGa_{1-x}As$ as a function of composition x. The solid line denotes the calculated average bandgap at various temperatures, and the dashed line denotes the conventional experimental bandgap. Each short horizontal gray bar symbols in (a) represent the bandgap of each configuration calculated using CE method. The colored symbols in (b) indicate the experimentally observed bandgap values.

fitted bandgap, which is indicated by the dashed line [12]. On the other hand, each short horizontal gray bar indicates the bandgap of each configuration, $E_{g,\sigma}$, which was calculated using the CE method and is identical to the value in Fig. 3. The calculated $\overline{E_g}$ values of the InAs-rich composition agree well with the experimental bandgap, but the discrepancy between the calculated and experimental values becomes larger as the composition becomes closer to GaAs, and finally, the calculated bandgap of GaAs is lower than the experimental counterpart by 0.14 eV. Although HSE06 is known to be better for calculating semiconductor bandgaps than conventional pseudopotentials, HSE06 has also been reported to underestimate GaAs bandgaps [22–24]. The calculated bandgap in Fig. 5(a) was rigidly shifted, as in previous reports, to improve the matching of the predicted bandgaps to the experimental values [25–28]. The amount of shifts was calculated by linearly interpolating the difference between the theoretical and experimental bandgaps of InAs and GaAs. The corrected calculated $\overline{E_g}$ in Fig. 5(b) agrees well with experimental data points denoted by colored symbols [11,29–31]. According to Eq. (3), a configuration with lower energy has higher P_σ. In combination with the inverse relationship between $E_{g,\sigma}$ and ΔE_σ presented in Fig. 3, a configuration with low energy and high P_σ has high $E_{g,\sigma}$, resulting in relatively high $\overline{E_g}$. However, the difference in P_σ between configurations with different energies decreases as the temperature increases. Owing to this fact, $\overline{E_g}$ tends to decrease as the temperature increases. The temperature dependency of the bandgaps caused by the configuration variation in this study did not take into account the lattice thermal expansion and electron–phonon interactions reported in some studies [32,33]. Fortunately, the fairly good agreement between the theoretical and experimental bandgaps in Fig. 5(b) implies the small electron–phonon coupling [34]. The calculation results reveal that ***P5Grand*** can successfully predict the ensemble-averaged bandgap of $In_xGa_{1-x}As$. Thus, ***P5Grand*** can be used to predict the arbitrary properties of pseudobinary systems by simply substituting the right input files for other PoIs.

4. Conclusion

This study introduces ***P5Grand***, which can predict thermodynamic properties (such as average energy, free energy, and phase diagram) and ensemble-averaged properties (such as bandgap and dielectric constant) while considering local compositional fluctuations that stochastically occur in pseudobinary systems. Its execution requires two input files: one file containing a set of compositions, energies, and PoIs as well as another file containing fitting parameters for strain energy. In this study, the temperature-dependent average bandgap of $In_xGa_{1-x}As$ was investigated as an application example of ***P5Grand***. The E_g and ΔE vary depending on the configuration and the composition, and a configuration with a higher bandgap tends to have lower mixing energy and vice versa. This inverse relationship between $E_{g,\sigma}$ and ΔE_σ of (In,Ga)As can be inferred from the opposite signs in the ECIs of E_g and ΔE. The $\overline{E_g}$ decreases as the temperature increases because of the inverse relationship between E_g and ΔE. ***P5Grand*** can be used to calculate various properties and phase diagrams of diverse pseudobinary systems, thereby assisting the community in designing solid solutions through computations.

CRediT authorship contribution statement

Gyuseung Han: Formal analysis, Investigation, Methodology, Software, Writing – original draft. **In Won Yeu:** Formal analysis, Writing – review & editing. **Kun Hee Ye:** Formal analysis, Writing – review & editing. **Seungjae Yoon:** Software, Writing – review & editing. **Taeyoung Jeong:** Writing – review & editing. **Seung-Cheol Lee:** Software, Writing – review & editing. **Cheol Seong Hwang:** Supervision, Writing – review & editing. **Jung-Hae Choi:** Conceptualization, Funding acquisition, Project administration, Supervision, Writing – review & editing.

Declaration of Competing Interest

The authors declare that they have no known competing financial interests or personal relationships that could have appeared to influence the work reported in this paper.

Acknowledgements

This work was supported by the National Research Foundation of Korea (NRF) grant funded by MSIT [2020R1A2C2003931], and by the Institutional Research Program of Korea Institute of Science and Technology (KIST) [2E31771]. The authors would also like to acknowledge the support from the KISTI Supercomputing Center through a Strategic Support Program for Supercomputing Application Research [KSC-2020-CRE-0236] and the provision of the cluster expansion package (LACOS) by Dr. Mahesh Chandran, former researcher at Indo-Korea Science and Technology Centre.

Appendix A. Supplementary material

Supplementary data to this article can be found online at https://doi.org/10.1016/j.cplett.2022.139887.

References

[1] T.F. Kuech, III-V compound semiconductors: growth and structures, Prog. Cryst. Growth Charact. Mater. 62 (2) (2016) 352–370, https://doi.org/10.1016/j.pcrysgrow.2016.04.019.

[2] Z. Li, J. Allen, M. Allen, H.H. Tan, C. Jagadish, L. Fu, Review on III-V semiconductor single nanowire-based room temperature infrared photodetectors, Materials (Basel) 13 (2020) 1400, https://doi.org/10.3390/ma13061400.

[3] C.-Z. Ning, L. Dou, P. Yang, Bandgap engineering in semiconductor alloy nanomaterials with widely tunable compositions, Nat. Rev. Mater. 2 (2017) 17070, https://doi.org/10.1038/natrevmats.2017.70.

[4] G. Han, I.W. Yeu, K.H. Ye, C.S. Hwang, J.-H. Choi, Atomistic prediction on the composition- and configuration-dependent bandgap of Ga(As, Sb) using cluster expansion and ab initio thermodynamics, Mater. Sci. Eng. B. 280 (2022) 115713, https://doi.org/10.1016/j.mseb.2022.115713.

[5] A. Zunger, S.-H. Wei, L.G. Ferreira, J.E. Bernard, Special quasirandom structures, Phys. Rev. Lett. 65 (3) (1990) 353–356, https://doi.org/10.1103/PhysRevLett.65.353.

[6] C.M. Andolina, P. Williamson, W.A. Saidi, Optimization and validation of a deep learning CuZr atomistic potential: Robust applications for crystalline and amorphous phases with near-DFT accuracy, J. Chem. Phys. 152 (15) (2020) 154701, https://doi.org/10.1063/5.0005347.

[7] C.M. Andolina, M. Bon, D. Passerone, W.A. Saidi, Robust, multi-length-scale, machine learning potential for Ag–Au bimetallic alloys from clusters to bulk materials, J. Phys. Chem. C 125 (31) (2021) 17438–17447, https://doi.org/10.1021/acs.jpcc.1c0440310.1021/acs.jpcc.1c04403.s001.

[8] C.M. Andolina, J.G. Wright, N. Das, W.A. Saidi, Improved Al-Mg alloy surface segregation predictions with a machine learning atomistic potential, Phys. Rev. Materials 5 (2021) 083804, https://doi.org/10.1103/PhysRevMaterials.5.083804.

[9] G. Han, I.W. Yeu, J. Park, K.H. Ye, S.-C. Lee, C.S. Hwang, J.-H. Choi, Effect of local strain energy to predict accurate phase diagram of III–V pseudobinary systems: case of Ga (As, Sb) and (In, Ga) As, J. Phys. D. Appl. Phys. 54 (4) (2021) 045104, https://doi.org/10.1088/1361-6463/abbf78.

[10] F.D. Murnaghan, The compressibility of media under extreme pressures, Proc. Natl. Acad. Sci. U. S. A. 30 (9) (1944) 244–247, https://doi.org/10.1073/pnas.30.9.244.

[11] J.C. Woolley, B.A. Smith, Solid solution in $A^{III}B^{V}$ compounds, Proc. Phys. Soc. 72 (2) (1958) 214–223, https://doi.org/10.1088/0370-1328/72/2/306.

[12] R.E. Nahory, M.A. Pollack, W.D. Johnston, R.L. Barns, Band gap versus composition and demonstration of Vegard's law for $In_{1-x}Ga_xAs_yP_{1-y}$ lattice matched to InP, Appl. Phys. Lett. 33 (7) (1978) 659–661, https://doi.org/10.1063/1.90455.

[13] E. Kuphal, Phase diagrams of InGaAsP, InGaAs and InP lattice-matched to (100) InP, J. Cryst. Growth. 67 (3) (1984) 441–457, https://doi.org/10.1016/0022-0248(84)90036-8.

[14] G. Kresse, J. Furthmüller, Efficiency of ab-initio total energy calculations for metals and semiconductors using a plane-wave basis set, Comput. Mater. Sci. 6 (1) (1996) 15–50, https://doi.org/10.1016/0927-0256(96)00008-0.

[15] G. Kresse, J. Furthmüller, Efficient iterative schemes for ab initio total-energy calculations using a plane-wave basis set, Phys. Rev. B. 54 (16) (1996) 11169–11186, https://doi.org/10.1103/PhysRevB.54.11169.

[16] I.W. Yeu, G. Han, J. Park, C.S. Hwang, J.-H. Choi, Theoretical understanding of the catalyst-free growth mechanism of GaAs <111>B nanowires, Appl. Surf. Sci. 497 (2019) 143740, https://doi.org/10.1016/j.apsusc.2019.143740.

[17] P.E. Blöchl, Projector augmented-wave method, Phys. Rev. B. 50 (24) (1994) 17953–17979, https://doi.org/10.1103/PhysRevB.50.17953.

[18] G. Kresse, D. Joubert, From ultrasoft pseudopotentials to the projector augmented-wave method, Phys. Rev. B. 59 (3) (1999) 1758–1775, https://doi.org/10.1103/PhysRevB.59.1758.

[19] J. Heyd, G.E. Scuseria, M. Ernzerhof, Hybrid functionals based on a screened Coulomb potential, J. Chem. Phys. 118 (18) (2003) 8207–8215, https://doi.org/10.1063/1.1564060.

[20] M. Chandran, Multiscale ab initio simulation of Ni-based alloys: Real-space distribution of atoms in $\gamma + \gamma'$ phase, Comput. Mater. Sci. 108 (2015) 192–204, https://doi.org/10.1016/j.commatsci.2015.06.029.

[21] S.B. Zhang, M.L. Cohen, High-pressure phases of III-V zinc-blende semiconductors, Phys. Rev. B. 35 (14) (1987) 7604–7610, https://doi.org/10.1103/PhysRevB.35.7604.

[22] M.A.L. Marques, J. Vidal, M.J.T. Oliveira, L. Reining, S. Botti, Density-based mixing parameter for hybrid functionals, Phys. Rev. B. 83 (2011) 35119, https://doi.org/10.1103/PhysRevB.83.035119.

[23] R.R. Pela, M. Marques, L.K. Teles, Comparing LDA-1/2, HSE03, HSE06 and G_0W_0 approaches for band gap calculations of alloys, J. Phys. Condens. Matter. 27 (50) (2015) 505502, https://doi.org/10.1088/0953-8984/27/50/505502.

[24] F. Viñes, O. Lamiel-García, K.C. Ko, J.Y. Lee, F. Illas, Systematic study of the effect of HSE functional internal parameters on the electronic structure and band gap of a representative set of metal oxides, J. Comput. Chem. 38 (11) (2017) 781–789, https://doi.org/10.1002/jcc.24744.

[25] C.-K. Tan, D. Borovac, W. Sun, N. Tansu, First-principle electronic properties of dilute-P $GaN_{1-x}P_x$ alloy for visible light emitters, Sci. Rep. 6 (2016) 1–9, https://doi.org/10.1038/srep24412.

[26] M. Zhang, X. Li, Structural and electronic properties of wurtzite $B_xAl_{1-x}N$ from first-principles calculations, Phys. Status Solidi. 254 (8) (2017) 1600749, https://doi.org/10.1002/pssb:v254.810.1002/pssb:201600749.

[27] F.W.Q. Almeida-Neto, G. Santos-Castro, M.B. da Silva, J.S. de Sousa, E.W. S. Caetano, P. Lima-Neto, V.N. Freire, Structural, electronic, and optical properties of inhomogeneous $Ca_{1-x}Mg_xO$ alloys, J. Appl. Phys. 125 (15) (2019) 155102, https://doi.org/10.1063/1.5053102.

[28] M. Jiang, H.Y. Xiao, S.M. Peng, L. Qiao, G.X. Yang, Z.J. Liu, X.T. Zu, Effects of stacking periodicity on the electronic and optical properties of GaAs/AlAs superlattice: a first-principles study, Sci. Rep. 10 (2020) 1–7, https://doi.org/10.1038/s41598-020-61509-x.

[29] E.F. Hockings, I. Kudman, T.E. Seidel, C.M. Schmelz, E.F. Steigmeier, Thermal and electrical transport in InAs-GaAs alloys, J. Appl. Phys. 37 (7) (1966) 2879–2887, https://doi.org/10.1063/1.1782144.

[30] G.A. Antypas, Liquid-phase epitaxy of $In_xGa_{1-x}As$, J. Electrochem. Soc. 117 (1970) 1393–1397, https://doi.org/10.1149/1.2407329.

[31] T.Y. Wu, G.L. Pearson, Phase diagram, crystal growth, and band structure of $In_xGa_{1-x}As$, J. Phys. Chem. Solids. 33 (2) (1972) 409–415, https://doi.org/10.1016/0022-3697(72)90022-4.

[32] W.A. Saidi, S. Poncé, B. Monserrat, Temperature dependence of the energy levels of methylammonium lead iodide perovskite from first-principles, J. Phys. Chem. Lett. 7 (24) (2016) 5247–5252, https://doi.org/10.1021/acs.jpclett.6b0256010.1021/acs.jpclett.6b02560.s001.

[33] J. Park, W.A. Saidi, J.K. Wuenschell, B.H. Howard, B. Chorpening, Y. Duan, Assessing the effects of temperature and oxygen vacancy on band gap renormalization in $LaCrO_{3-\delta}$: first-principles and experimental corroboration, ACS Appl. Mater. Interfaces 13 (15) (2021) 17717–17725, https://doi.org/10.1021/acsami.1c0350310.1021/acsami.1c03503.s001.

[34] A. Martinez, A. Price, R. Valin, M. Aldegunde, J. Barker, Impact of phonon scattering in Si/GaAs/InGaAs nanowires and FinFets: a NEGF perspective, J. Comput. Electron. 15 (4) (2016) 1130–1147, https://doi.org/10.1007/s10825-016-0851-0.